Structural insight into Ca^{2+} specificity in tetrameric cation channels

Amer Alam, Ning Shi, and Youxing Jiang*

Department of Physiology, University of Texas Southwestern Medical Center, Dallas, TX 75390-9040

Communicated by Roderick MacKinnon, The Rockefeller University, New York, NY, August 3, 2007 (received for review July 5, 2007)

Apparent blockage of monovalent cation currents by the permeating blocker Ca^{2+} is a physiologically essential phenomenon relevant to cyclic nucleotide-gated (CNG) channels. The recently determined crystal structure of a bacterial homolog of CNG channel pores, the NaK channel, revealed a Ca^{2+} binding site at the extracellular entrance to the selectivity filter. This site is not formed by the side-chain carboxylate groups from the conserved acidic residue, Asp-66 in NaK, conventionally thought to directly chelate Ca^{2+} in CNG channels, but rather by the backbone carbonyl groups of residue Gly-67. Here we present a detailed structural analysis of the NaK channel with a focus on Ca^{2+} permeability and blockage. Our results confirm that the Asp-66 residue, although not involved in direct chelation of Ca^{2+}, plays an essential role in external Ca^{2+} binding. Furthermore, we give evidence for the presence of a second Ca^{2+} binding site within the NaK selectivity filter where monovalent cations also bind, providing a structural basis for Ca^{2+} permeation through the NaK pore. Compared with other Ca^{2+}-binding proteins, both sites in NaK present a novel mode of Ca^{2+} chelation, using only backbone carbonyl oxygen atoms from residues in the selectivity filter. The external site is under indirect control by an acidic residue (Asp-66), making it Ca^{2+}-specific. These findings give us a glimpse of the possible underlying mechanisms allowing Ca^{2+} to act both as a permeating ion and blocker of CNG channels and raise the possibility of a similar chemistry governing Ca^{2+} chelation in Ca^{2+} channels.

calcium blockage | cyclic nucleotide-gated channel pore | NaK channel | nonselective cation channel

Cyclic nucleotide-gated (CNG) channels play an essential role in signal transduction pathways of visual and olfactory sensory systems, among others (1–4). Generally nonspecific for Group 1A monovalent cations, CNG channels also allow the passage of divalent cations like Ca^{2+} and Mg^{2+}, albeit at much slower rates, through their pores. This, in turn, leads to an effective blockage of monovalent currents (5–14). Ca^{2+} blockage from the extracellular side, a property central to the physiological functioning of CNG channels (1), has been extensively studied by using electrophysiological tools and is thought to arise primarily from the involvement of a conserved acidic residue, usually glutamate, in the selectivity filter of the CNG channel (14–17). Mutating this residue to a neutral amino acid has been shown to drastically decrease external Ca^{2+} blockage, whereas substituting glutamate with aspartate preserved it. In the absence of structural information, it was previously speculated that the four conserved acidic residues of the channel tetramer, one from each subunit, point their side chains toward the ion conduction pathway and directly chelate a Ca^{2+} ion with their carboxylate oxygen atoms.

The recently discovered NaK channel from *Bacillus cereus* provides a viable structural model for analyzing Ca^{2+} permeation in CNG channels. NaK has a selectivity filter sequence of $_{63}$TVGDG$_{67}$ similar to that of CNG channels [supporting information (SI) Fig. 7], and it exhibits similar ion conduction properties. NaK conducts various monovalent cations (18), and monovalent cation conduction can be reduced by divalent cations (SI Fig. 8). A discrete Ca^{2+} binding site at the extracellular entrance to the pore was observed in the crystal structure of NaK, revealing a possible structural basis for external divalent cation blockage in CNG channels (Fig. 1). Contrary to expectations based on the mutagenesis of CNG channels, the conserved acidic residue in the NaK filter (Asp-66) does not directly bind Ca^{2+}. Instead, the four backbone carbonyl oxygen atoms of Gly-67, one from each subunit, chelate the Ca^{2+} ion. The side chain of Asp-66 actually points away from the ion conduction pathway with its carboxylate group positioned at the opposite side of the Ca^{2+}-binding carbonyl group of Gly-67 and very close to the amide nitrogen of the peptide bond between Gly-67 and Gln-68. Here we performed an extensive crystallographic study of the NaK channel and its mutants to analyze their Ca^{2+} permeability and blockage properties, with a particular focus on the role of Asp-66 in specific Ca^{2+} binding at the extracellular entrance. Our results reveal a mechanism underlying specific Ca^{2+} binding in NaK, which most likely also applies to CNG channels.

Results

Extracellular Ca^{2+} Binding in D66E and D66N Mutants. To test whether the conserved acidic residue (Asp-66) in the NaK filter is important for Ca^{2+} binding, similar to what has been observed in CNG channels, mutant NaK channels were generated in which Asp-66 was substituted with glutamate (D66E) and asparagine (D66N). By using ^{86}Rb flux assays, these mutants were shown to conduct monovalent cations like the wild-type channel, indicating that the respective mutations did not affect the ion conduction properties of NaK (data not shown). Both the D66E and D66N mutants were crystallized in the presence of 200 mM $CaCl_2$ and their structures were determined at 2.6 Å and 2.4 Å, respectively (*Materials and Methods* and SI Table 1) and shown to be virtually identical to wild type. However, strong electron density of a bound Ca^{2+} ion at the external entrance of the filter was present in the D66E mutant, as in wild type (Fig. 2 *A* and *B*) but absent in the D66N structure (Fig. 2 *C* and *D*), indicating a loss of external Ca^{2+} binding. The bound ion at the external entrance of the D66E filter was confirmed to be Ca^{2+} through soaking experiments which showed it is replaceable by Ba^{2+} but not monovalent cations (Rb^+ or Cs^+) (SI Fig. 9). Ca^{2+} binding at the external site therefore seems to be mediated primarily by the preservation of charge rather than side chain size. We also note that, in contrast to wild-type and D66E mutant channels,

Author contributions: A.A. and Y.J. designed research; A.A. performed research; A.A., N.S., and Y.J. analyzed data; and A.A. and Y.J. wrote the paper.

The authors declare no conflict of interest.

Abbreviation: CNG, cyclic nucleotide-gated.

Data deposition: The atomic coordinates have been deposited in the Protein Data Bank, www.pdb.org [PDB ID codes 2Q67 (D66A), 2Q68 (D66AS70E), 2Q69 (D66N0), and 2Q6A (D66E)].

*To whom correspondence should be addressed at: Department of Physiology, University of Texas Southwestern Medical Center, 5323 Harry Hines Boulevard, Dallas, TX 75390-9040. E-mail: youxing.jiang@utsouthwestern.edu.

This article contains supporting information online at www.pnas.org/cgi/content/full/0707324104/DC1.

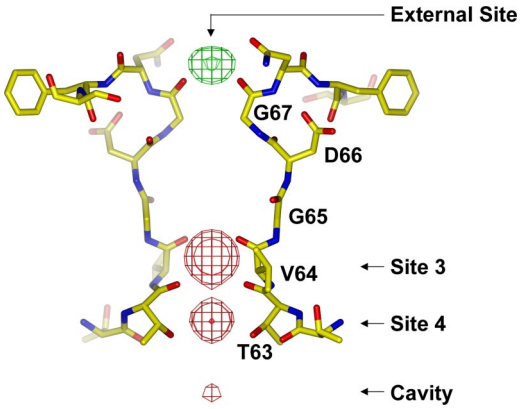

Fig. 1. Structure of the NaK selectivity filter (PDB ID code 2AHY) with an $F_o - F_c$ ion omit map contoured at 8 σ indicating the bound ions (green mesh for Ca^{2+} and red for Na^+).

residues forming the entrance to the pore region (residues 65–68) in the D66N mutant appear to have become more disordered (Fig. 2*C*), suggesting that Ca^{2+} binding to the entryway might rigidify the local structure.

Extracellular Ca^{2+} Binding in D66AS70E and D66A. The D66E and D66N mutant structural data suggests that the presence of a negative charge in close proximity to the peptide bond between Gly-67 and Asn-68 is essential to mediate Ca^{2+} binding at the external site. To further test this hypothesis we designed a double mutant channel, D66AS70E, in which Asp-66 was replaced by alanine and Ser-70 was replaced by glutamate. The double mutant structure was determined at 2.5 Å (SI Table 1) and revealed the carboxylate group from the original Asp-66 residue replaced by one from Glu-70 of a neighboring subunit (Fig. 3*A*). Consistent with our hypothesis, strong Ca^{2+} ion density was observed at the pore entrance in both $2F_o - F_c$ and $F_o - F_c$ ion omit maps (Fig. 3 *A* and *B*). The presence of a bound Ca^{2+} ion at this site was further confirmed by soaking experiments performed with other monovalent (Rb^+ and Cs^+) and divalent (Ba^{2+}) cations (SI Fig. 10). As a control, the structure of an D66A mutant channel also was determined at 2.3 Å (SI Table 1). Interestingly, Ca^{2+} binding was still observed in this structure (Fig. 3 *C* and *D*) which, as discussed below, turned out to be much weaker than that observed in the wild-type, D66E, and D66AS70E channels. A closer inspection of the D66A structure revealed an ordered water molecule in the exact location of the missing Asp-66 carboxylate group (Fig. 3*C*). A partial negative charge on this water molecule could weakly compensate for the missing negative charge contributed by Asp-66 and, combined with the high concentration of Ca^{2+} in the crystallization conditions, likely accounts for the observed Ca^{2+} binding in the D66A mutant.

Relative Ca^{2+} Binding Affinities in Wild-Type and Mutant NaK Channels. For a comparison of relative Ca^{2+} binding affinities in the wild-type and different mutant channels, we soaked the respective protein crystals in stabilization solutions containing lower concentrations of Ca^{2+} (10 mM and 1 mM; *see Materials and Methods*). Fig. 4 *A* and *B* presents $F_o - F_c$ ion omit maps generated from crystals subjected to these titration experiments. At 10 mM Ca^{2+}, density of externally bound Ca^{2+} was present in wild type and in the D66E and D66AS70E mutants but not observed in the D66A mutant (Fig. 4*A*). At 1 mM Ca^{2+}, Ca^{2+} density became weak in wild type and in the D66AS70E mutant but remained strong in the D66E mutant, indicating higher Ca^{2+} binding affinity in D66E (Fig. 4*B*). The density of bound Ca^{2+} in D66E was shown to be abolished by soaking the crystals in a solution containing no Ca^{2+} (with 5 mM EGTA; data not shown). A number of important conclusions can be drawn from this crystallographic titration assay. First, the loss of Ca^{2+} binding at 10 mM Ca^{2+} concentration confirms that Ca^{2+} binding in the D66A mutant is very weak. Second, the results not only provide a qualitative picture of the relative Ca^{2+} affinities among wild-type and mutant channels, which follows the sequence D66E > wild type ≈ D66AS70E > D66A > D66N, but they also provide further support for the hypothesis that the

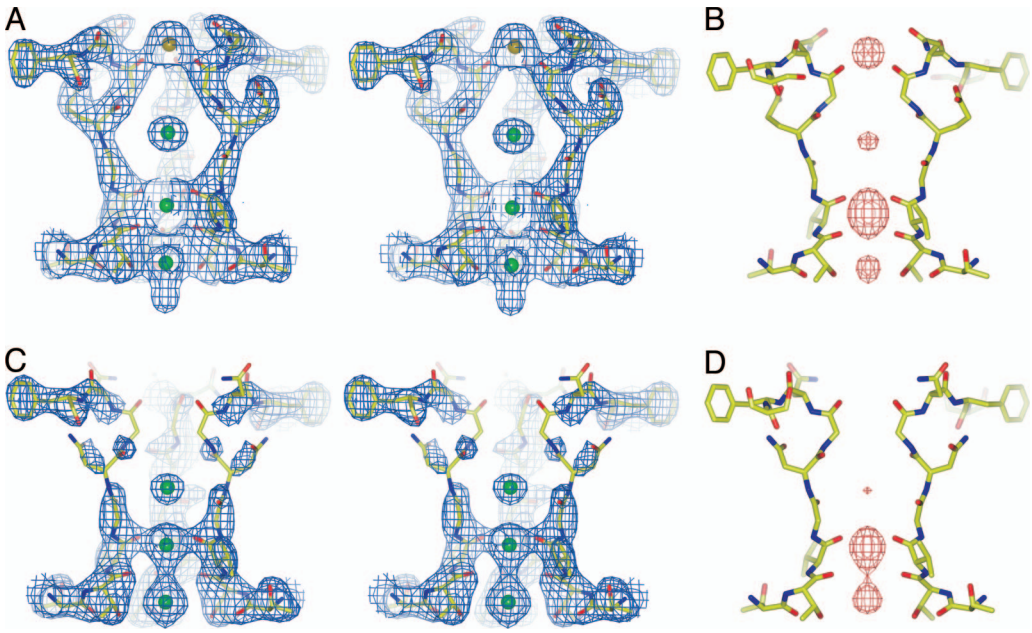

Fig. 2. Structural analysis of NaK D66E and D66N mutants. (*A*) Stereoview of a $2F_o - F_c$ map (1.5 σ) of D66E at the filter region. The bound Ca^{2+} ion is modeled as an orange sphere. (*B*) An $F_o - F_c$ ion omit map (8 σ) at the D66E filter. (*C*) Stereoview of a $2F_o - F_c$ map (1.5 σ) of D66N at the filter region. (*D*) An $F_o - F_c$ ion omit map (8 σ) at the D66N filter.

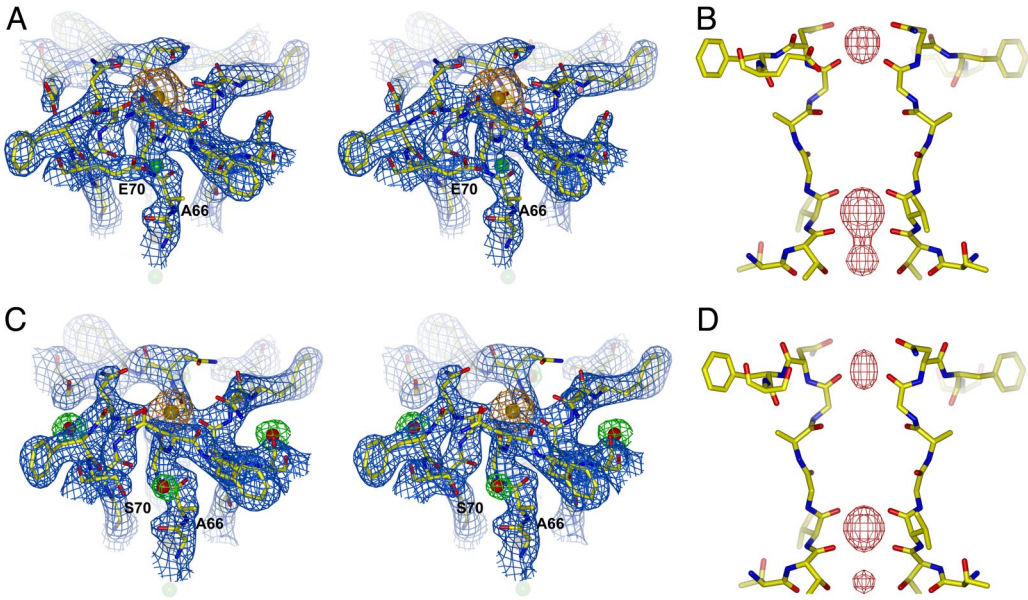

Fig. 3. Structural analysis of NaK D66AS70E and D66A mutants. (*A*) A $2F_o - F_c$ map (1.5 σ) of the D66AS70E mutant around the external Ca^{2+} binding site. The density and sphere model of the Ca^{2+} ion are colored orange. (*B*) An $F_o - F_c$ ion omit map (8 σ) at the D66AS70E filter. (*C*) A $2F_o - F_c$ map (1.5 σ) of the D66A mutant around the Ca^{2+} binding site. The density and sphere model of the Ca^{2+} ion are colored orange. Density for water molecules (red spheres) is colored green. (*D*) An $F_o - F_c$ ion omit map (8 σ) at the D66A filter. Also see Fig. 6*A* for a close-up view of mutant NaK channels focused on the region surrounding residue 66.

presence of negative charge in the vicinity of Gly-67 plays the determinant role in Ca^{2+} binding. Finally, the reduction and eventual loss of electron density at lower Ca^{2+} concentrations further confirms the specificity of the external site for divalent cations.

Second Ca^{2+} Binding Site Within the NaK Selectivity Filter. An interesting and physiologically significant property of CNG channels is their ability to conduct Ca^{2+} in addition to monovalent cations. Functional studies of Ca^{2+} permeation and blockage in CNG channels have pointed to the presence of multiple Ca^{2+} binding sites (7, 15, 19, 20). This prompted us to look for evidence of Ca^{2+} binding elsewhere in the NaK filter in addition to the external site. Site 3 in the NaK channel was previously shown by soaking experiments to bind Ba^{2+} in addition to monovalent cations (19), suggesting that Ca^{2+} might also bind here. A second indication of Ca^{2+} binding at site 3 arose from a closer analysis of the Na^+ and K^+ complex structures of NaK (SI Table 2). The Na^+ complex structure revealed much stronger electron density of bound ions at site 3 than at site 4 (Fig. 5*A*), whereas, in the K^+ complex, structure electron density at both sites was roughly equivalent, with the density at site 4 being marginally stronger (Fig. 5*B*). Furthermore, we also determined the Rb^+ complex structure of NaK at 2.6 Å, which revealed noticeably stronger electron density at site 4 than at site 3 (Fig. 5*C*). Taking into account the number of electrons in these various cations (Na^+ = 10e, K^+ = Ca^{2+} = 18e, and Rb^+ = 36e) and the fact that monovalent cations bind at both sites 3 and 4 (based on previous soaking experiments), we predict that the observed differences in relative intensity of the electron density at sites 3 and 4 could arise from Ca^{2+} (the only other cation present in crystallization conditions) binding at site 3 in addition to monovalent cations. To confirm this, we purified the NaK channel in LiCl, crystallized it in the presence of 200

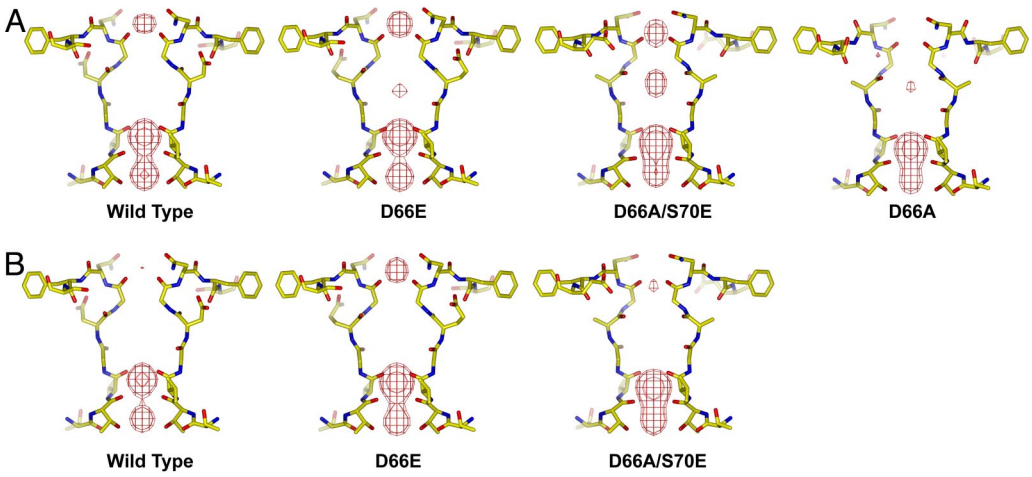

Fig. 4. Titration analysis of Ca^{2+} affinity in NaK and its mutants. Shown are the $F_o - F_c$ ion omit maps (6 σ) of wild-type and mutant channel crystals soaked in stabilization solution containing 10 mM (*A*) and 1 mM (*B*) Ca^{2+}.

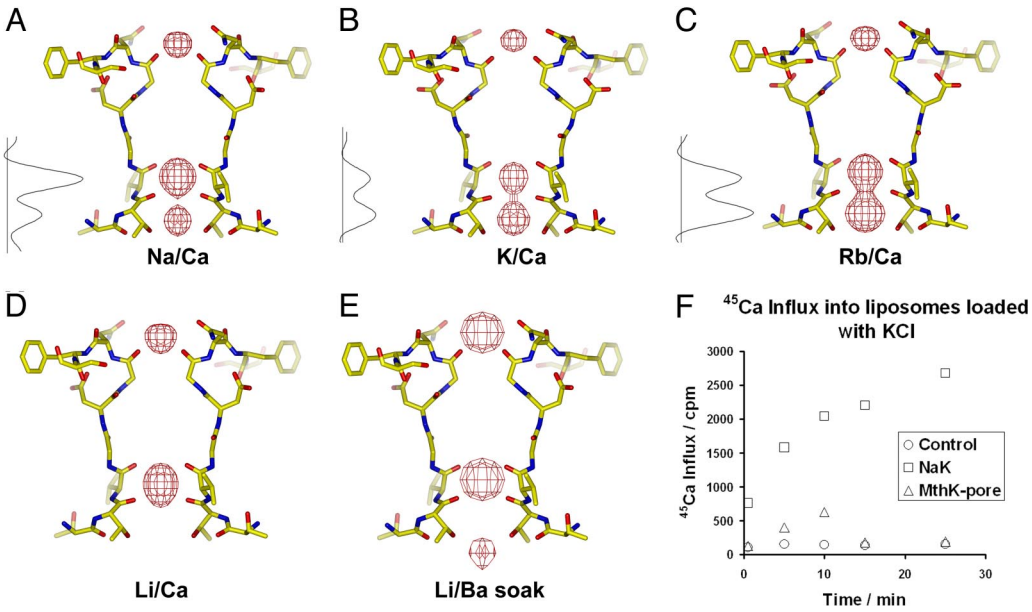

Fig. 5. Structural study of NaK channels crystallized in the presence of different monovalent cations. All crystallization conditions contain 200 mM $CaCl_2$. Shown are $F_o - F_c$ ion omit maps (8 σ) at the filter region calculated from crystals grown in the presence of 100 mM concentrations of NaCl (2.4 Å) (*A*), KCl (2.8 Å) (*B*), RbCl (2.6 Å) (*C*), and LiCl (2.5 Å) (*D*). The maps of Na^+ and K^+ complexes were calculated from previously determined structures with the PDB ID codes 2AHY and 2AHZ, respectively. One-dimensional electron density profiles of bound ions at sites 3 and 4 in Na^+, K^+, and Rb^+ complexes were obtained by sampling the $F_o - F_c$ ion omit maps along the central axis of the filter. (*E*) An $F_{soak} - F_{reference}$ difference map (8σ) at 3.2 Å between crystal grown in LiCl/$CaCl_2$ (reference) and crystal soaked in LiCl/$BaCl_2$ (soak). (*F*) Time-dependent ^{45}Ca influx into liposomes loaded with 400 mM KCl and reconstituted with NaKNΔ19, MthK pore, and no protein (as control).

mM $CaCl_2$, and determined its structure at 2.5 Å (SI Table 2). As shown in the $F_o - F_c$ ion omit map, in addition to the external entrance of the pore, strong electron density also was observed at site 3 (Fig. 5*D*). Because the Li^+ ion has only two electrons, this strong density must come from a bound Ca^{2+} ion. Site 4 did not reveal any such density, indicating that Ca^{2+} binds preferably to site 3 within the NaK filter. Difference maps calculated from the Li^+ complex crystals soaked in a solution containing $BaCl_2$ gave rise to strong density at the external entrance and site 3, indicating that both Ca^{2+} ions can be replaced by Ba^{2+} (Fig. 5*E*). Although not a direct measurement of Ca^{2+} permeation in NaK, the structural observation that Ca^{2+} binds deep in the selectivity filter in addition to the external site raises the possibility of the NaK channel, like CNG channels, being permeable to Ca^{2+}.

Monitoring Ca^{2+} Permeation in NaK by Using ^{45}Ca Flux Assays. NaK has so far proven to be averse to electrophysiological analysis, possibly because of a low open probability and/or conductance. Additionally, the ^{86}Rb flux assay used for initial analysis of ion conduction in NaK is not sensitive enough to measure Ca^{2+} permeation in NaK, nor can this assay distinguish between internal and external blockage of NaK by Ca^{2+}. We therefore measured the uptake of Ca^{2+} directly in liposomes loaded with 400 mM KCl and reconstituted with NaKNΔ19, a truncated form of NaK lacking the N-terminal 19 residues. The method is similar to the ^{86}Rb flux assays except that ^{45}Ca is used as the radioactive tracer (see *Materials and Methods*). Results from these ^{45}Ca flux assays show time-dependent accumulation of ^{45}Ca in liposomes containing NaK but not in control liposomes containing either no reconstituted protein or the K^+ conducting MthK pore (21), indicating that NaK likely conducts Ca^{2+} (Fig. 5*F*). The activity of the reconstituted proteins also was analyzed by ^{86}Rb flux assays, which showed strong, time-dependent accumulation of ^{86}Rb in liposomes reconstituted with NaKNΔ19 or the MthK pore (data not shown), confirming that both had the ability to conduct K^+ and build up the required membrane potential for influx of ^{86}Rb or ^{45}Ca. These data, along with our structural studies, which were guided by functional and mutational analyses of Ca^{2+} permeation and blockage in CNG channels, offer a plausible structural basis for the so called "permeating block" associated with Ca^{2+} permeability.

Discussion

Ca^{2+} binding motifs in most known Ca^{2+} binding proteins, although diverse, use oxygen atoms contributed by carboxylate, carbonyl, and hydroxyl groups, as well as water molecules, as ligands (22, 23). Additionally, side chain carboxylate groups are always seen to act as ligands and most likely play a part in balancing the Ca^{2+} ion's positive charge. The mode of Ca^{2+} chelation in NaK, however, appears to be unique. The ion is chelated at both sites in the NaK pore exclusively by backbone carbonyl oxygen atoms rather than the carboxylate oxygen atoms of acidic residues. Only the external site is Ca^{2+}-specific, and our data suggest that this specificity arises from a through-space interaction between the Asp-66 side chain and Gly-67 backbone carbonyl group, most likely electrostatic in nature, which helps generate a highly favorable environment for Ca^{2+} chelation by the latter. A close-up view of the region immediately surrounding residue 66 in NaK and its mutants (D66E, D66AS70E, and D66A) provides a plausible explanation for the specificity of external Ca^{2+} binding in NaK that most likely applies to CNG channels also (Fig. 6*A*). A common feature among these NaK channels is the close proximity of the amide nitrogen atom of the Gly-67/Asn-68 peptide bond and the negatively charged oxygen atom from the side chain carboxylate group (Asp-66 in wild type, Glu-66 in the D66E mutant, and Glu-70 in the D66AS70E mutant) or partially charged oxygen atom from the water molecule in the D66A mutant. In our view, using the wild-type channel as an example, the most likely scenario places the negatively charged carboxylate oxygen atom of Asp-66 close enough to the amide nitrogen of the Gly-67/Asn-68 peptide bond to stabilize its double bonded resonance form through a salt-

BIOPHYSICS

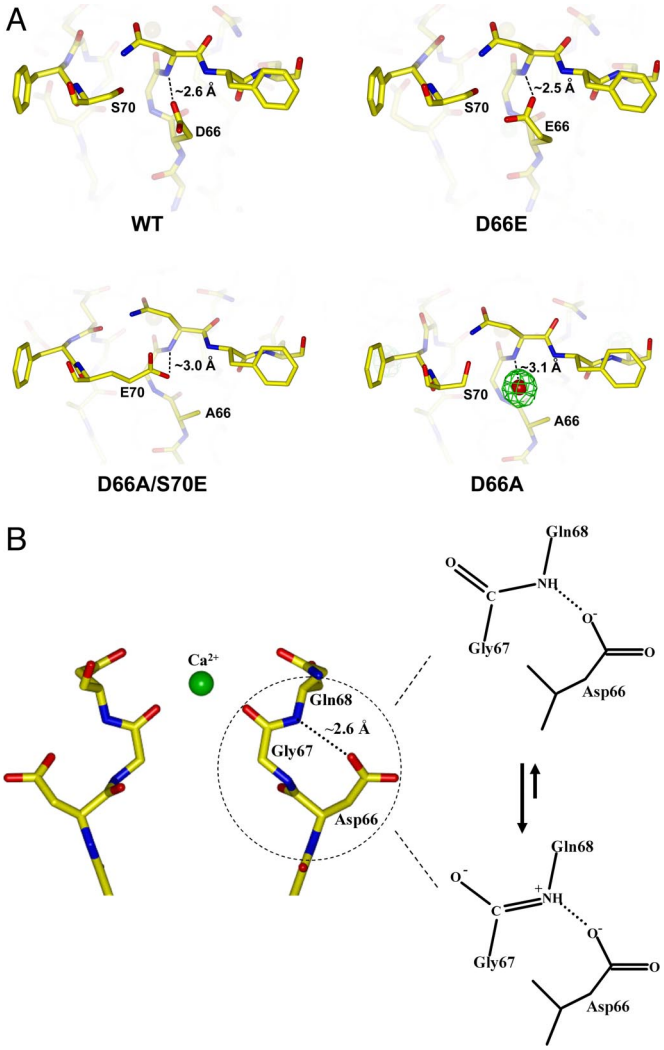

Fig. 6. Mechanism for the specificity of external Ca^{2+} binding in NaK. (*A*) Close-up view of wild-type and mutant NaK channels at the region surrounding residue 66. In wild type and in the D66E mutant, the carboxylate oxygen atoms from D66 or E66 form hydrogen bond interactions with the amide nitrogen of the Gly-67/Asn-68 peptide bond. In the D66A/S70E double mutant, the carboxylate oxygen of E70 from the neighboring subunit forms a similar hydrogen bond interaction with the same amide nitrogen. In D66A, a water molecule (red sphere with green mesh representing its electron density) sits at the same position as the carboxylate group in the wild-type channel and interacts with the amide nitrogen. Distances between the amide nitrogen of the Gly-67/Asn-68 peptide bond and the oxygen atoms involved in the hydrogen bond interaction are indicated. (*B*) Proposed mechanism underlying specific Ca^{2+} binding at the external entrance of the NaK filter mediated by the nearby acidic residue Asp-66.

bridge-like interaction (Fig. 6*B*). This, in turn, places a negative charge on the backbone carbonyl oxygen atom of Gly-67 from each channel monomer, making it a more suitable ligand for Ca^{2+}. Our data also suggest that Ca^{2+} likely permeates the channel by subsequently binding to another intrapore binding site, site 3, which lacks the involvement of any acidic residues and is therefore nonspecific and able to bind monovalent cations.

The mechanism discussed above, whereby the properly positioned carboxylate group of Asp-66, instead of binding Ca^{2+} directly, appears to confer Ca^{2+} specificity to the external Ca^{2+} binding site, has intriguing implications for Ca^{2+} selectivity in Ca^{2+} channels, suggested to occur through similar mechanisms as those in CNG channels (2, 4). It is likely that Ca^{2+} channels also use backbone carbonyl groups to bind Ca^{2+} whereas the four acidic residues of the EEEE locus, shown by mutagenesis to be the sole element determining Ca^{2+} selectivity (24–26), confer Ca^{2+} specificity through similar mechanisms as seen here in NaK. This model is more readily reconciled with the plethora of evidence suggesting that Ca^{2+} channels have multi-ion pores when compared with concurrent views of a single, flexible, and rapidly rearranging Ca^{2+} binding site formed by the EEEE locus (27).

Materials and Methods

Protein Preparation and Crystallization. All genes encoding wild-type and mutant NaK channel proteins were cloned into the pQE60 expression vector and expressed in *Escherichia coli* XL1-Blue cells. NaK mutants were generated by QuikChange site-directed mutagenesis (Strategene, La Jolla, CA). Proteins were purified as tetramers in *n*-decyl-β-D-maltoside (DM) with NaCl, RbCl, or LiCl present as the monovalent salt. Crystals of wild-type and mutant channels were grown by using the sitting drop vapor diffusion method at 20°C by mixing equal volumes of protein (30–35 mg/ml) and reservoir solution containing 200 mM $CaCl_2$, 100 mM Tris·HCl (pH 8.0), 37–42% PEG 400, and 4% *tert*-butanol. All crystals were of space group $C222_1$ with similar unit cell dimensions (SI Tables 1 and 2).

Crystal Soaking Experiments. Mutant NaK crystals were soaked in stabilization solutions containing 40% PEG 400, 100 mM Tris·HCl (pH 8.0), 20 mM DM, 4% *tert*-butanol, 100 mM XCl, and 200 mM YCl_2, where X and Y represent a monovalent cation (Na^+, Rb^+, or Cs^+) and a divalent cation (Ca^{2+} or Ba^{2+}), respectively. To minimize nonisomorphism, data from the respective mutant crystals soaked in a stabilization solution containing 100 mM NaCl and 200 mM $CaCl_2$ was used as reference data, against which all data from other soaked crystals were merged and scaled. For the titration analysis of Ca^{2+} affinity, the respective crystals were soaked in stabilization solutions containing 40% PEG 400, 100 mM Tris·HCl (pH 8.0), 20 mM DM, 4% *tert*-butanol, 500 mM NaCl, and 1 or 10 mM $CaCl_2$. The structures of those crystals used in the titration experiments were refined to resolutions between 2.8 Å and 3.1 Å.

Data Collection and Structure Determination. All data were collected at the Advanced Photon Source and processed with HKL2000 (28). Structures were determined by rigid-body refinement using the Na^+ complex structure of NaK as the initial model followed by iterative cycles of simulated annealing with torsion-angle dynamics in CNS (29) and model rebuilding in O (30). Detailed statistics of data collection and refinement are listed in SI Tables 1 and 2. All ion omit difference maps using Fourier coefficients ($F_o - F_c$) were calculated with phases from refined models that contained no ions in the selectivity filters.

Protein Reconstitution and Flux Assays. The MthK pore and NaKNΔ19 constructs were purified as described previously (18, 21). The proteins were reconstituted in lipid vesicles composed of a 3:1 ratio of 1-palmitoyl-2-oleoyl-phosphatidylethanolamine and 1-palmitoyl-2-oleoyl-phosphatidylglycerol at a protein/lipid ratio of 6 and 10 μg/mg, respectively, as described previously (31), with the following modifications: 10 mM DM was used to solubilize the lipid and dialysis [against a reconstitution buffer of 10 mM Hepes (pH 7.4), 400 mM KCl, and 4 mM *N*-methyl-D-glucamine] was used to slowly remove the detergent from the detergent/lipid/protein mixture. The reconstituted liposome samples were kept at −80°C in 100-μl aliquots.

^{86}Rb flux assays were performed as described previously (18, 32) except that gel filtration through a prespun Sephadex G-50 fine resin soaked in 400 mM sorbitol/4 mM *N*-methyl-D-glucamine/10 mM Hepes, pH 7.4 (buffer A), was used to remove extraliposomal ^{86}Rb before measuring radioactivity levels in liposomes. ^{45}Ca flux assays were performed similarly to the ^{86}Rb

flux assays except that ^{45}Ca was used as the radioactive tracer and buffer A was supplemented with 5 mM $CaCl_2$.

Use of the Argonne National Laboratory Structural Biology Center beamlines at the Advanced Photon Source was supported by the U.S. Department of Energy, Office of Energy Research. We thank the beamline staff for assistance in data collection. This work was supported by grants from the David and Lucile Packard Foundation and the McKnight Foundation. A.A. was supported by National Institutes of Health Training Grant T32 GM008297.

1. Yau KW, Baylor DA (1989) *Annu Rev Neurosci* 12:289–327.
2. Kaupp UB, Seifert R (2002) *Physiol Rev* 82:769–824.
3. Matulef K, Zagotta WN (2003) *Annu Rev Cell Dev Biol* 19:23–44.
4. Zagotta WN, Siegelbaum SA (1996) *Annu Rev Neurosci* 19:235–263.
5. Baumann A, Frings S, Godde M, Seifert R, Kaupp UB (1994) *EMBO J* 13:5040–5050.
6. Finn JT, Solessio EC, Yau KW (1997) *Nature* 385:815–819.
7. Frings S, Seifert R, Godde M, Kaupp UB (1995) *Neuron* 15:169–179.
8. Hackos DH, Korenbrot JI (1999) *J Gen Physiol* 113:799–818.
9. Picones A, Korenbrot JI (1995) *Biophys J* 69:120–127.
10. Haynes LW, Kay AR, Yau KW (1986) *Nature* 321:66–70.
11. Stern JH, Knutsson H, MacLeish PR (1987) *Science* 236:1674–1678.
12. Colamartino G, Menini A, Torre V (1991) *J Physiol* 440:189–206.
13. Zimmerman AL, Baylor DA (1992) *J Physiol* 449:759–783.
14. Seifert R, Eismann E, Ludwig J, Baumann A, Kaupp UB (1999) *EMBO J* 18:119–130.
15. Root MJ, MacKinnon R (1993) *Neuron* 11:459–466.
16. Eismann E, Muller F, Heinemann SH, Kaupp UB (1994) *Proc Natl Acad Sci USA* 91:1109–1113.
17. Gavazzo P, Picco C, Eismann E, Kaupp UB, Menini A (2000) *J Gen Physiol* 116:311–326.
18. Shi N, Ye S, Alam A, Chen L, Jiang Y (2006) *Nature* 440:570–574.
19. Karpen JW, Brown RL, Stryer L, Baylor DA (1993) *J Gen Physiol* 101:1–25.
20. Dzeja C, Hagen V, Kaupp UB, Frings S (1999) *EMBO J* 18:131–144.
21. Li Y, Berke I, Chen L, Jiang Y (2007) *J Gen Physiol* 129:109–120.
22. Katz AK, Glusker JP, Beebe SA, Bock CW (1996) *J Am Chem Soc* 118:5752–5763.
23. Pidcock E, Moore GR (2001) *J Biol Inorg Chem* 6:479–489.
24. Tang S, Mikala G, Bahinski A, Yatani A, Varadi G, Schwartz A (1993) *J Biol Chem* 268:13026–13029.
25. Ellinor PT, Yang J, Sather WA, Zhang JF, Tsien RW (1995) *Neuron* 15:1121–1132.
26. Yang J, Ellinor PT, Sather WA, Zhang JF, Tsien RW (1993) *Nature* 366:158–161.
27. Sather WA, McCleskey EW (2003) *Annu Rev Physiol* 65:133–159.
28. Otwinowski Z, Minor W (1997) *Methods Enzymol* 276:307–326.
29. Brunger AT, Adams PD, Clore GM, DeLano WL, Gros P, Grosse-Kunstleve RW, Jiang JS, Kuszewski J, Nilges M, Pannu NS, *et al*. (1998) *Acta Crystallogr D* 54:905–921.
30. Jones TA, Zou JY, Cowan SW, Kjeldgaard (1991) *Acta Crystallogr A* 47:110–119.
31. Heginbotham L, LeMasurier M, Kolmakova-Partensky L, Miller C (1999) *J Gen Physiol* 114:551–560.
32. Heginbotham L, Kolmakova-Partensky L, Miller C (1998) *J Gen Physiol* 111:741–749.